ACSNANO

www.acsnano.org

ARTICLE

Strategies for the Site-Specific Decoration of DNA Origami Nanostructures with Functionally Intact Proteins

Joschka Hellmeier,* René Platzer, Vanessa Mühlgrabner, Magdalena C. Schneider, Elke Kurz, Gerhard J. Schütz, Johannes B. Huppa, and Eva Sevcsik*

Cite This: *ACS Nano* 2021, 15, 15057−15068

Read Online

ACCESS | Metrics & More | Article Recommendations | Supporting Information

ABSTRACT: DNA origami structures provide flexible scaffolds for the organization of single biomolecules with nanometer precision. While they find increasing use for a variety of biological applications, the functionalization with proteins at defined stoichiometry, high yield, and under preservation of protein function remains challenging. In this study, we applied single molecule fluorescence microscopy in combination with a cell biological functional assay to systematically evaluate different strategies for the site-specific decoration of DNA origami structures, focusing on efficiency, stoichiometry, and protein functionality. Using an activating ligand of the T-cell receptor (TCR) as the protein of interest, we found that two commonly used methodologies underperformed with regard to stoichiometry and protein functionality. While strategies employing tetravalent wildtype streptavidin for coupling of a biotinylated TCR-ligand yielded mixed populations of DNA origami structures featuring up to three proteins, the use of divalent (dSAv) or DNA-conjugated monovalent streptavidin (mSAv) allowed for site-specific attachment of a single biotinylated TCR-ligand. The most straightforward decoration strategy, *via* covalent DNA conjugation, resulted in a 3-fold decrease in ligand potency, likely due to charge-mediated impairment of protein function. Replacing DNA with charge-neutral peptide nucleic acid (PNA) in a ligand conjugate emerged as the coupling strategy with the best overall performance in our study, as it produced the highest yield with no multivalent DNA origami structures and fully retained protein functionality. With our study we aim to provide guidelines for the stoichiometrically defined, site-specific functionalization of DNA origami structures with proteins of choice serving a wide range of biological applications.

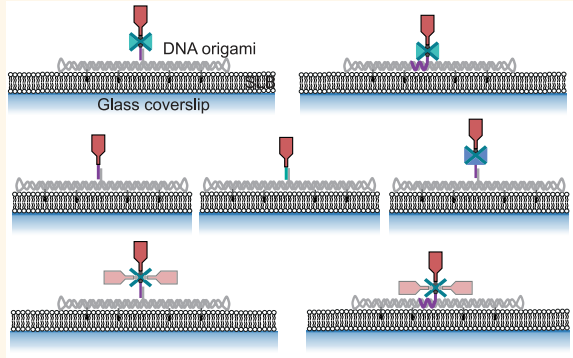

KEYWORDS: *DNA origami, DNA nanostructures, protein conjugation, functionalization, single molecule fluorescence microscopy, T-cell activation*

DNA origami nanotechnology has emerged as a versatile tool for interrogating biological processes at a molecular and mechanistic level. By using short oligonucleotides ("staples") to guide the folding of a long single stranded DNA scaffold, it is possible not only to program the shape of a DNA origami structure but also to arrange functional elements with nanometer resolution and precision.[1] Protein-decorated DNA origami structures have thus far been interfaced with cells as soluble agents,[2,3] attached to a solid substrate,[4,5] or anchored to a fluid supported lipid bilayer (SLB);[6,7] biological questions addressed range from studying cellular signaling and adhesion processes,[2−6,8,9] to creating synthetic multienzyme cascades[10,11] to more and more elaborate robotic DNA machines.[12]

The self-assembly of the DNA origami structures is typically straightforward. However, the challenge lies in their functionalization with proteins at defined stoichiometries with high yield while preserving protein function. A commonly applied method involves covalent conjugation of an oligonucleotide to a specific site within a protein of interest (reviewed in ref 13) followed by hybridization to a complementary elongated staple strand (handle) on the DNA origami structure. The highly negatively charged DNA phosphate backbone, however, has been observed to affect functionalization yield[14,15] as well as

Received: June 24, 2021
Accepted: August 26, 2021
Published: August 31, 2021

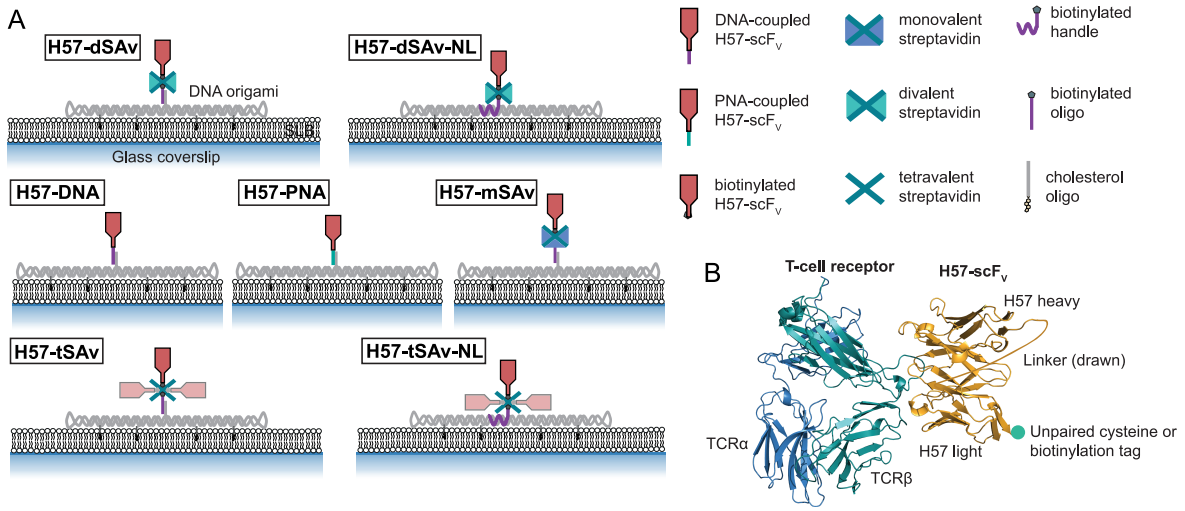

Figure 1. Strategies for site-specific functionalization of DNA origami with a single chain antibody fragment. (A) The single chain antibody fragment derived from the TCR*β*-reactive mAb H57 (H57-scF$_V$) was site-specifically attached to the DNA origami tile *via* different strategies. (B) Model based on a TCR−H57 Fab structure (PDB: 1NFD). At the C-terminus, the H57-scF$_V$ was equipped with either an unpaired cysteine or an Avi-tag for site-specific biotinylation *via* birA.

enzyme activity.[16−19] Genetically encoded protein tags[20,21] or DNA-binding proteins[22] allow for a defined stoichiometry and highly specific binding but require the generation of fusion proteins and often suffer from low coupling yields,[15,23] attributable to electrostatic repulsion between the DNA origami structure and protein of interest.[14] Alternatively, streptavidin (SAv) has been frequently used as a connector to attach biotinylated proteins to the DNA origami structure *via* a biotinylated handle.[5,23−26] This strategy has the advantage of shielding the protein from the negatively charged DNA. However, given the tetravalency of SAv for biotin-binding, single sites on the DNA origami may get functionalized with up to three proteins resulting in a stoichiometrically ill-defined product. While this may be acceptable for some applications, many mechanistic studies, for example, those focusing on receptor−ligand interactions,[2,3,6] depend on the functionalization with not more than one protein at a specific site. We have recently circumvented this potential shortcoming of streptavidin by using divalent SAv (dSAv)[27] as a connector to strictly avoid double or triple occupancies at a single modification site.[6]

As protein-functionalized DNA origami structures are becoming widely accessible research tools for the mechanistic study of diverse biophysical and cell biological processes, there is an increased need for robust methods to reliably produce high-quality DNA origami constructs. To date, however, systematic studies which provide the basis for the informed choice of a functionalization method are missing. With this work we offer a guideline for the site-specific, stoichiometrically defined functionalization of DNA origami structures with a protein of interest, with a particular focus on preserving full protein functionality. To this end, we systematically examined and optimized two commonly used approaches for the site-specific attachment of proteins to DNA origami structures, that is, *via* commercially available streptavidin and DNA−protein conjugates, and introduced adaptations to these strategies to improve their performance. Specifically, we determined (i) the yield of DNA origami structures functionalized with one (or more) proteins (functionalization efficiency), as well as (ii) the number of proteins per functionalized DNA origami structure (functionalization stoichiometry) by using single molecule fluorescence microscopy. We chose an activating ligand of the T-cell receptor (TCR) for functionalization, which allowed us to assess (iii) protein functionality by monitoring its stimulatory capacity in the presence of T-cells. In total, we compared seven different attachment strategies based on mono-, di-, and tetravalent streptavidin as well as covalent conjugation *via* DNA and PNA oligonucleotides (Figure 1A). While functionalization efficiencies for all tested strategies ranged from 67 to 74%, the use of tetravalent streptavidin did not yield stoichiometrically defined functionalization, which markedly affected the functional response to the ligand-decorated DNA origami constructs. Interestingly, the most straightforward approach for ligand coupling, using a DNA-ligand conjugate, markedly compromised ligand functionality. A strategy employing PNA instead of DNA for ligand conjugation gave rise to the best overall performance in our study, as it produced the highest yield of 74% with no multivalent DNA origami structures and fully retained protein functionality.

RESULTS AND DISCUSSION

For the quantitative comparison of different functionalization strategies, we employed a recently introduced platform[6] based on rectangular DNA origami tiles anchored to a fluid-phase supported lipid bilayer (SLB) *via* cholesterol-modified oligonucleotides.[28] DNA origami constructs were assembled from a 65 × 54 nm DNA origami tile[1] featuring a centrally located and elongated staple strand to create a target for quantitative functionalization with protein (Supporting Information, Figure S1). As protein of interest, we selected for this study a monovalent single-chain antibody fragment of the variable domain derived from the TCR*β*-reactive monoclonal antibody H57-597 (H57-scF$_V$),[29] which was shown to induce T-cell activation when displayed on SLBs.[6,30] We further equipped the H57-scF$_V$ C-terminally with either a biotin ligase recognition sequence or an unpaired cysteine for the site-specific attachment to DNA origami structures, that would not interfere with TCR binding (Figure 1B). All functionalization steps were carried out in solution followed by attachment of

https://doi.org/10.1021/acsnano.1c05411
ACS Nano 2021, 15, 15057−15068

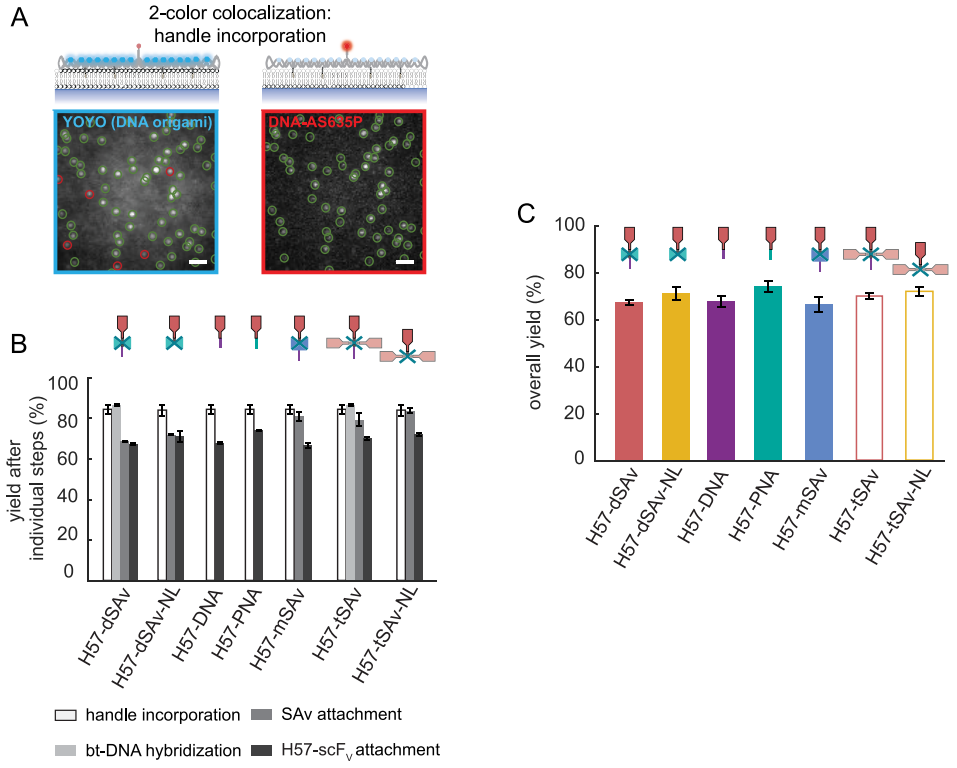

Figure 2. DNA origami functionalization efficiencies for the different site-specific attachment strategies. (A) Single molecule two-color colocalization TIRF imaging of DNA origami structures on a SLB was applied to determine the efficiency of each modification step. Determination of the incorporation efficiency of a fluorescently labeled handle (DNA-AS635P) in the DNA origami tile (labeled with the DNA-intercalating fluorophore YOYO) is shown as an example. Green open circles indicate signals detected in both color channels; red open circles indicate signals detected only in one channel. The percentage of colocalized signals in the blue (YOYO) and the red (DNA-AS635P) color channel amount to the efficiency of handle incorporation. (B) The functionalization efficiency after each step was determined *via* two-color colocalization microscopy (see Figures S3−S9). (C) Functionalization yields of DNA origami structures with H57-scF$_V$ are displayed. For each construct, data represent the mean of at least two independent experiments (±s.e.m.).

the fully assembled DNA origami constructs to a fluid SLB *via* cholesterol-modified oligonucleotides. Of note, all SLB-anchored DNA origami constructs exhibited free Brownian motion with a diffusion constant of ∼0.38 $\mu m^2/s$ (Figure S2, Table S1).

To determine the efficiency of individual functionalization steps, we used single molecule two-color colocalization total internal reflection fluorescence (TIRF) microscopy (Figure 2A, Table S2). By varying molar ratios and incubation times, optimum conditions for each functionalization step were determined and then applied as the basis for subsequent steps (Figures S3−S9; Tables S3−S9). First, we determined the incorporation efficiency of the handle into the DNA origami tile. For this purpose, we employed a handle conjugated to Abberior Star 635P (DNA-AS635P) and labeled the DNA origami structure randomly with the DNA-intercalating fluorophore YOYO-1 iodide (YOYO). Two-color colocalization analysis of single molecule localizations recorded in the blue color channel (YOYO) with single molecule localizations recorded in the red color channel (DNA-AS635P) revealed an incorporation efficiency of ∼84% (Figure 2B), which is in good agreement with previously reported values for the center of a 2D DNA origami tile.[31] Note that this value represents a conservative estimate, as substoichiometric labeling of the DNA-AS635P, fluorophore bleaching during recording, and fluorophores present in the dark state were not taken into account.

We have previously used a strategy in which a biotinylated oligonucleotide was hybridized to the handle on the DNA origami tile followed by the attachment of divalent streptavidin (dSAv)[27] and biotinylated Alexa Fluor 555 (AF555)-labeled H57-scF$_V$ (H57-dSAv, Figure 1A). This approach requires three additional functionalization steps following the incorporation of the handle (Figure S3); we determined the yield after each of these steps by two-color colocalization microscopy (Figure 2B). By optimizing the molar ratios and incubation times (Table S3), we could increase the previously reported overall yield of ∼60%[6] to ∼67% (Figure 2C, Table S10). Furthermore, our results reveal that the availability of the handle and the efficiency of the subsequent modification steps contribute to a similar extent to the overall degree of functionalization. Note that two-color colocalization microscopy yields the efficiency of functionalization with at least one ligand. To assess the extent to which this was equal to *exactly one* ligand (strict 1:1 stoichiometry), we next determined the number of ligands per DNA origami construct by comparing the signal brightness of the construct to the brightness of a single AF555-labeled H57-scF$_V$. As shown in Figure 3A, virtually all localizations corresponded to single H57-scF$_V$ molecules (Figure S10; Table S11).

The functionalization strategy *via* dSAv as described above has several advantages. It reduces unwanted interactions between ligand and DNA, ensures a 1:1 stoichiometry of functionalization, and is cost-efficient and versatile, as the same biotinylated oligonucleotide can be used for introducing a

https://doi.org/10.1021/acsnano.1c05411
ACS Nano 2021, 15, 15057−15068

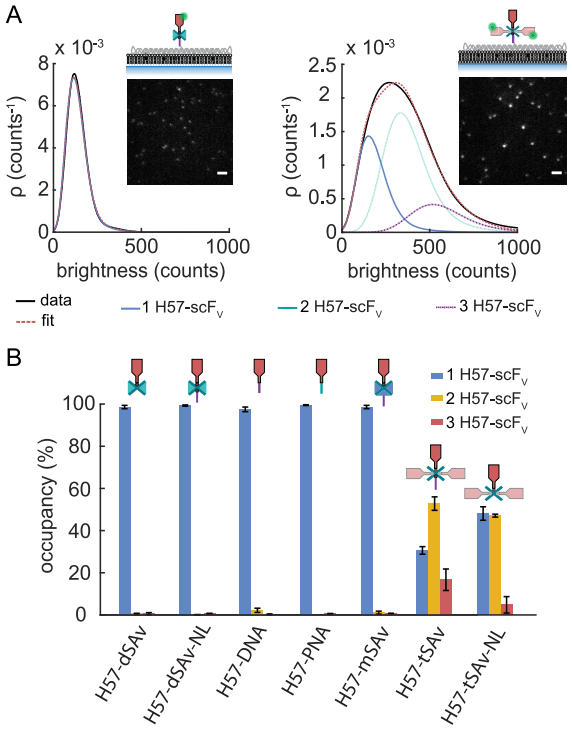

Figure 3. DNA origami functionalization stoichiometry for the different attachment strategies. (A) The number of H57- scF$_V$s per DNA origami structure was determined *via* single molecule brightness analysis. Representative TIRF images (insets) and the corresponding brightness distributions ρ of biotinylated and AF555-conjugated scF$_V$s bound *via* dSAv (H57-dSAv, left) and tSAv (H57-tSAv, right) to DNA origami structures on SLBs are shown. The detected signals were fitted and the brightness distribution was deconvolved into monomer and multimer contributions[48] (see methods section). Scale bar, 2 μm. (B) The percentage of detected (i.e., ligand-functionalized) DNA origami structures carrying 1, 2, or 3 H57-scF$_V$s as determined from single-molecule brightness analysis. Means of at least two independent experiments are shown (±s.e.m.).

functionalization site at various positions on the DNA origami tile by merely changing the position of the handle. The latter aspect, however, comes at a cost: stable hybridization of the biotinylated oligo to the handle requires at least 16 base pairs[32,33] (we have used 17 nucleotides in this study), creating a double stranded DNA linker between DNA origami and dSAv with a length of ∼7 nm (SI Figure S11). This, in turn, has several consequences that need to be considered: (i) The DNA linker is connected to the DNA origami tile *via* four unpaired bases, thus conferring a certain degree of flexibility to the ligand which at the same time reduces the positional accuracy with respect to the DNA origami tile. (ii) The linker increases the axial distance between the SLB-anchored DNA origami and the ligand, which may affect interactions that are sensitive to force and intermembrane distance. In the construct H57-dSAv-NL (no linker), we thus employed a short, biotinylated staple strand to directly attach dSAv to the DNA origami tile, which is expected to position the biotinylated ligand at a distance of ∼4 nm from the DNA origami surface, thus permitting a lower degree of motional freedom compared to the longer dsDNA linker present in construct H57-dSAv (SI Figure S4). This attachment strategy resulted in a slightly higher functionalization yield (Figure 2B,C).

Next, we determined whether the presence of the linker had an effect on the potency of the DNA origami constructs to activate T-cells. For this purpose, T-cells were confronted with SLBs presenting DNA origami constructs at different ligand surface densities together with His-tagged adhesion (ICAM-1) and co-stimulatory (B7−1) molecules as described previously.[6] For each experiment, the surface density of H57-scF$_V$ on SLBs was assessed by relating the average fluorescence signal per area to the brightness of a single AF555-labeled H57-scF$_V$ molecule. To monitor T-cell activation, T-cells were labeled with the calcium-sensitive dye Fura-2 AM, seeded onto DNA origami/SLB surfaces (Figure 4A) and the level of intracellular calcium was assessed *via* ratiometric imaging (Figure S12). The percentage of activated cells was determined for each SLB, plotted as a dose−response curve (Figure 4B) and fitted with eq 19 to determine H57-scF$_V$ densities at half-maximal response hereafter referred to as "activation threshold". All fit parameters are listed in Table S12. For H57-dSAv-NL we determined an activation threshold of ∼3 H57-scF$_V$ per μm^2 (Figure 4C), similar to the value we had previously reported for H57-dSAv,[6] indicating that the dsDNA linker in the DNA origami construct did not markedly affect the potency of the TCR-ligand to activate T-cells.

Although the individual steps for functionalizing the dSAv constructs were rather efficient, each modification step may be a source of error. Another drawback of strategies employing dSAv is that they do not allow the attachment of different ligands to create heterofunctional DNA origami structures. To address this limitation, we generated an H57-scF$_V$-DNA conjugate by coupling a 17 base oligonucleotide to the free cysteine at the C-terminus of the H57-scF$_V$ (see methods section for details) and attached it directly to the complementary handle on the DNA origami tile *via* in-solution hybridization (H57-DNA, Figure 1A, Figure S5) at an efficiency of ∼80%, yielding a total coupling efficiency of ∼68% (Figure 2B,C). We found, however, that ligand functionality was considerably reduced, as evidenced by a 3-fold increased activation threshold (10 μm^{-2} compared to 3 μm^{-2} for H57-dSAv-NL, Figure 4B,C). Conjugation of DNA oligonucleotides has been reported to affect enzyme activity,[16−19] possibly due to local pH-changes or distinct contacts between nucleic and amino acids. Considering the rather small size of H57-scF$_V$ (27 kDa) it seemed conceivable that direct coupling of the highly negatively charged DNA oligonucleotide interfered with TCR binding. Indeed, while soluble, unmodified H57-scF$_V$ binds the TCR with high affinity at ∼95% labeling efficiency,[29] which amounted to a surface density of ∼95 H57-scF$_V$-labled TCRs per μm^2 on the T-cell surface, we found that TCR staining by H57-DNA was markedly reduced (∼20 H57-scF$_V$-labled TCRs per μm^2) (Figure S13).

Considering the detrimental effect of the negatively charged DNA tag on ligand activity, we decided to use a PNA oligo as a charge-neutral alternative.[34] The PNA backbone is composed of repeating peptide-like amide units (*N*-(2-aminoethyl) glycine), thereby supporting high-affinity PNA−DNA duplex formation due to the absence of interstrand electrostatic repulsion. In a recent study, to our knowledge the only one employing PNA for functionalization of DNA origami thus far, a ligand conjugated with a PNA oligonucleotide of only nine bases was efficiently coupled to a DNA handle on a DNA origami structure.[3] Indeed, H57-scF$_V$ functionality could be completely restored by substituting the DNA oligo with PNA

https://doi.org/10.1021/acsnano.1c05411
ACS Nano 2021, 15, 15057−15068

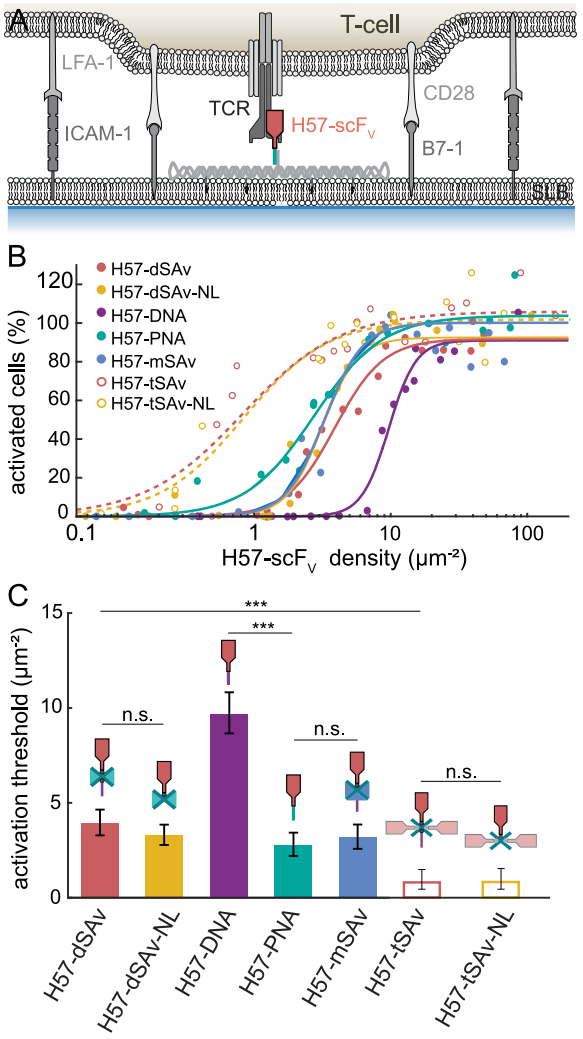

Figure 4. Ligand coupling strategy affects T-cell activation. (A) T-cells were interfaced with SLBs featuring ligand-decorated DNA origami constructs, adhesion (ICAM-1) and co-stimulatory molecules (B7−1). (B) Dose−response curves for T-cell activation mediated by H57-scF$_V$ presented in the context of the different DNA origami constructs. Each data point corresponds to the percentage of activated cells determined in an individual experiment at a specific H57-scF$_V$ density. Data were normalized to activation levels recorded for a positive control (=100%) involving the use of SLBs featuring His-tagged pMHC (His-pMHC) at a density of 150 μm^{-2} and His-tagged ICAM-1 and B7−1 at 100 μm^{-2}. Dose−response curves were fitted with eq 19 (see methods section) to extract activation thresholds (C). For each dose−response curve, data are from at least two independent experiments involving T-cells isolated from two different mice. For details we refer to SI Table S12. Error bars represent the 95% confidence interval.

(H57-PNA, Figure S6), giving rise to an activation threshold of 2.5 H57-scF$_V$ molecules per μm^2 (Figure 4B,C) as well as a higher hybridization efficiency of 88%, and thus a total functionalization efficiency of ∼74%. (Figure 2B,C; Table S10). Accordingly, soluble H57-PNA labeled TCRs on the T-cell surface with a similar efficiency when compared to unconjugated or biotinylated H57-scF$_V$ (SI Figure S13).

To combine the advantages of streptavidin-based strategies (i.e., use of a biotinylated protein, avoidance of electrostatic interactions between DNA and the protein of interest) and hybridization-based strategies (i.e., creation of heterofunctional DNA origami), we introduced a DNA-conjugated monovalent tetrameric streptavidin (mSAv) as a spacer protein, which was attached to the DNA origami tile *via* hybridization to the handle, followed by coupling of a site-specifically biotinylated H57-scF$_V$ to the mSAv (H57-mSAv, Figure S7). Indeed, using mSAv to shield the H57-scF$_V$ from the negatively charged DNA fully restored ligand functionality (Figure 4B,C) at a total coupling yield of 67% (Figure 2C) and a defined 1:1 stoichiometry (Figure 3B).

The attachment strategies described so far require biochemical expertise and instrumentation which may not be accessible in every lab. While ensuring stoichiometrically well-defined binding, neither mSAv nor dSAv are readily available. Instead, commercially available tetravalent streptavidin (tSAv) has often been used, and while it offers in principle three sites for ligand binding, only one may be accessible due to steric hindrance when surface-attached.[35] Differences in the cellular response to a ligand presented *via* mSAv and tSAv have been observed yet attributed to the presence of a flexible linker in the mSAv construct.[7] To assess biochemical and functional consequences of tSAv valency in more detail, we designed the construct H57-tSAv in analogy to H57-dSAv but replaced the divalent with tetravalent streptavidin (Figure S8). While showing similar functionalization efficiency (Figure 2B,C), this strategy yielded a mixed population, with detected DNA origami constructs featuring one (∼30%), two (∼53%), and three ligands (∼17%) as determined *via* single molecule brightness analysis (Figure 3A,B, Table S11).

In a previous study, we had found that the lateral spacing of H57-scF$_V$ dramatically affected T-cell activation.[6] The presentation of two H57-scF$_V$ ligands at spacings below 20 nm resulted in substantially increased potency compared to ligand spacings of ≥48 nm, as enforced by the DNA origami tiles also used in the present study (Figure 4B,C). Indeed, the H57-tSAv construct yielded an activation threshold of ∼0.3 μm^{-2}, almost 1 order of magnitude lower than the strictly monovalent constructs and similar to the value we had previously determined for divalent constructs. It hence appears likely that at least two of the three tSAv-bound H57-scF$_V$s, that are maximally available per DNA origami, participate in TCR binding.

The binding geometry of H57-scF$_V$ to the TCR[29] renders the ligand perpendicular to the SLB; that is, H57-scF$_V$ bound to the trans binding pocket of tSAv, most effective for TCR binding. In an attempt to decrease the availability of the two biotin binding pockets adjacent to the one used for attachment to the DNA origami tile, we omitted the dsDNA linker in construct H57-tSAv-NL to attach tSAv closer to the DNA origami surface (Figure S9). While this configuration significantly reduced triple occupancies (to ∼5%), still half of all signals originated from DNA origami tiles carrying two H57-scF$_V$s (Figure 3B). Accordingly, H57-tSAv-NL activated T-cells with high potency (Figure 4B), indicating that our efforts to decrease the availability of the second tSAv-bound H57 for TCR binding were not successful. While functionalization with larger proteins would likely increase the fraction of monovalent DNA origami structures due to steric hindrance, we consider it unlikely that a strictly monovalent population can be achieved using tSAv for attachment. Given that exact placement of proteins within DNA origami structures is a primary reason for their use in the first place, this obvious lack of experimental control diminishes the usefulness of tetravalent

https://doi.org/10.1021/acsnano.1c05411
ACS Nano 2021, 15, 15057−15068

streptavidin in many biological and biophysical applications. In fact, we have previously observed that the presence of only 0.5% DNA origami structures carrying two H57-scF$_V$s at a distance of 10 nm instead of a single H57-scF$_V$ dominates T-cell activation behavior[6] with obvious consequences for the kind of conclusions that can be drawn from such experiments.

CONCLUSION

We have here systematically evaluated and optimized strategies for site-specific protein functionalization of DNA origami structures on the example of the TCR-ligand H57-scFv, with the aim of presenting guidelines tailored toward different experimental capacities and requirements. Focusing particularly on functionalization stoichiometry and protein functionality, we found that two commonly used methodologies underperformed with regard to these critical aspects: covalent conjugation of a DNA oligonucleotide and subsequent hybridization to the DNA origami structure resulted in a 3-fold decreased ligand potency. For strategies employing tetravalent streptavidin, on the other hand, the majority of DNA origami structures were functionalized with more than one biotinylated protein at a single modification site, rendering this approach inadequate if the anticipated experiment mandates a defined stoichiometry of target protein to allow for a conclusive outcome.

The use of charge neutral PNA oligos for protein conjugation emerged as the strategy with the best overall performance in our study, as it produced the highest coupling yield of 74% with no multivalent DNA origami structures and fully retained protein functionality. Moreover, PNA-based functionalization is well suited for creating heterofunctionalized DNA origami that carry several different proteins of interest. A versatile and less cost-intensive alternative to PNA conjugation at a slightly lower yield was the use of DNA-conjugated mSAv and a biotinylated protein, where SAv acted as spacer to the negatively charged DNA. Similar to direct protein conjugation of DNA or PNA oligonucleotides, this strategy allows the generation of heterofunctional DNA origami structures by preincubating the proteins of interest with mSAv prior to hybridization. In conclusion, PNA- and mSAv-based strategies are highly valuable for the site-specific protein functionalization of DNA origami structures and for serving a wide range of biological applications.

MATERIALS AND METHODS

Assembly of DNA origami tiles. DNA origami structures were assembled in a single folding reaction carried out in a test tube (AB0620, ThermoFisher Scientific) with 10 μL of folding mixture containing 10 nM M13mp18 scaffold DNA (New England Biolabs), 100 nM unmodified oligonucleotides (Integrated DNA technologies), either 100 nM biotin-modified oligonucleotides (Biomers) for direct hybridization to the DNA origami tile (H57-dSAv-NL, H57-tSAv-NL) or 500 nM biotinylated oligonucleotides (Biomers) for external hybridization (H57-dSAv, H57-tSAv) and folding buffer (5 mM Tris (AM9855G, ThermoFisher Scientific), 50 mM NaCl (AM9759, ThermoFisher Scientific), 1 mM EDTA (AM9260G, ThermoFisher Scientific), 12.5 mM MgCl2) (AM9530G, ThermoFisher Scientific)). Oligonucleotide sequences are shown in the Supporting Information Appendix, Tables S13–S15. At the site chosen for ligand attachment, a staple strand was elongated at its 3′-end with 21 bases (H57-DNA, H57-PNA, H57-mSAv, H57-dSAv, H57-tSAv). At sites chosen for cholesterol anchor attachment, staple strands were elongated at the 5′-end with 25 bases, respectively. DNA origami were annealed using a thermal protocol (90 °C, 15 min; 90 °C − 4 °C, 1 °C min^{-1}; 4 °C, 6 h) and purified using 100 kDa Amicon Ultra centrifugal filters (UFC510096, Merck). DNA origami were stored up to 4 weeks at −20 °C.

Functionalization of DNA Origami Tiles. In the following, assembly strategies are given at optimal conditions for each construct. For further details regarding the individual functionalization steps, we refer to Figures S3–S9. Functionalized DNA origami constructs were not stored but used for experiments on the same day.

Construct 1: H57-dSAv. For H57-dSAv, DNA origami were functionalized in a three-step assembly process (Figure S3). A biotinylated oligonucleotide was hybridized at 5× molar excess to a protruding elongated staple strand during the initial thermal annealing process of the DNA origami tile followed by purification using 100 kDa AmiconUltra centrifugal filters (Merck). In a next step, DNA origami structures were incubated with a 10× molar excess of dSAv for 30 min at 24 °C, and excessive dSAv was removed using 100 kDa AmiconUltra centrifugal filters. As a last step, AF555-conjugated and site-specifically biotinylated H57-scF$_V$ was added at a 10× molar excess for 60 min at 24 °C. Finally, H57-scF$_V$ not bound to DNA origami structures was removed using 100 kDa AmiconUltra centrifugal filters.

Construct 2: H57-dSAv-NL. For H57-dSAv-NL, DNA origami were functionalized in a three-step assembly process (Figure S4). At the site chosen for ligand attachment, the staple strand was modified with a biotin group and added at a 10× molar excess to the DNA origami folding mix during the initial thermal annealing process followed by purification. Next, DNA origami were incubated with a 10× molar excess of dSAv for 60 min at 24 °C, and excessive dSAv was removed using 100 kDa AmiconUltra centrifugal filters. AS635P-conjugated and site-specifically biotinylated H57-scF$_V$ was added at a 10× molar excess for 60 min at 24 °C. Finally, excessive H57-scF$_V$ was removed using 100 kDa AmiconUltra centrifugal filters.

Construct 3: H57-DNA. For H57-DNA, DNA origami were functionalized in a two-step assembly process (SI Figure S5). Here, the AF555-conjugated H57-scF$_V$ was site-specifically modified with a complementary DNA strand (DNA-H57) (see below) and hybridized to the elongated staple strand on the DNA origami tile. For functionalization, DNA origami were incubated with a 10× molar excess of DNA-H57 for 60 min at 35 °C and cooled down to 4 °C at 1 °C min^{-1}. Excessive DNA-H57 was removed during a final purification step using 100 kDa AmiconUltra centrifugal filters.

Construct 4: H57-PNA. For H57-PNA, DNA origami were functionalized in a two-step assembly process (Figure S6). For this purpose, the AF555-conjugated H57-scF$_V$ was site-specifically modified with a complementary PNA strand (PNA-H57) and hybridized to the elongated staple strand on the DNA origami tile. For functionalization, DNA origami were incubated with a 3× molar excess of PNA-H57 for 60 min at 35 °C and cooled down to 4 °C at 1 °C min^{-1}. Excessive PNA-H57 was removed during a final purification step using 100 kDa AmiconUltra centrifugal filters.

Construct 5: H57-mSAv. For H57-mSAv, DNA origami were functionalized in a three-step assembly process (Figure S7). For this purpose, a complementary DNA oligo was conjugated to a free cysteine on mSAv (DNA-mSAv) (see below) and hybridized to the elongated staple strand on the DNA origami tile. For this, DNA origami were incubated with a 3× molar excess of DNA-mSAv for 60 min at 35 °C and cooled down to 4 °C at 1 °C min^{-1}. Excessive DNA-mSAv was removed using 100 kDa AmiconUltra centrifugal filters. Finally, AF555-conjugated and site-specifically biotinylated H57-scF$_V$ was added at a 10× molar excess for 60 min at 24 °C, followed by a final purification step to remove excessive H57-scF$_V$.

Construct 6: H57-tSAv. For H57-tSAv, DNA origami were functionalized in a three-step assembly process (Figure S8) similarly to H57-dSAv. A biotinylated oligonucleotide was hybridized at 5× molar excess to the complementary elongated staple strand on the DNA origami tile during the initial thermal annealing process followed by purification. In a next step, DNA origami were incubated with a 10× molar excess of tSAv for 30 min at 24 °C. Excessive tSAv was removed using 100 kDa AmiconUltra centrifugal filters. Further, AF555-conjugated and site-specifically biotinylated H57-scF$_V$ was

https://doi.org/10.1021/acsnano.1c05411
ACS Nano 2021, 15, 15057−15068

added at a 10× molar excess for 60 min at 24 °C. Finally, excessive H57-scF$_V$ was removed using 100 kDa AmiconUltra centrifugal filters.

Construct 7:H57-tSAv-NL. For H57-tSAv-NL, DNA origami were functionalized in a three-step assembly process (Figure S9) in analogy to H57-dSAv-NL.

Preparation of Functionalized Planar SLBs. For DNA origami characterization, vesicles containing 100% 1-palmitoyl-2-oleoyl-sn-glycero-3-phosphocholine (POPC) (Avanti Polar Lipids) were prepared at a total lipid concentration of 0.5 mg mL^{-1} as described[29] in 10× Dulbecco's phosphate-buffered saline (PBS) (D1408-500ML, Sigma-Aldrich). Glass coverslips (# 1.5, 24 mm × 60 mm, Menzel) were plasma cleaned for 10 min and attached with the use of dental imprint silicon putty (Picodent twinsil 22, Picodent) to Lab-Tek 8-well chambers (ThermoFisher Scientific), from which the glass bottom had been removed.[36] Coverslips were incubated with a 5-fold diluted vesicle solution for 10 min, before they were extensively rinsed with PBS (D1408-500ML, Sigma-Aldrich). For functionalization, SLBs were first incubated for 60 min with cholesterol-modified oligonucleotides (Integrated DNA technologies) complementary to the elongated staple strands at the bottom side of the DNA origami and then rinsed with PBS. DNA origami were incubated on SLBs in PBS + 1% BSA (A9418-10G, Sigma-Aldrich) for 60 min. For T-cell activation experiments, vesicles containing 98% 1-palmitoyl-2-oleoyl-*sn*-glycero-3-phosphocholine (POPC) and 2% 1,2-dioleoyl-*sn*-glycero-3-[*N*(5-amino-1-carboxypentyl) iminodiacetic acid]succinyl[nickel salt] (Ni-DOGS NTA) (Avanti Polar Lipids) were used, and SLBs were formed as described above. Upon incubation of DNA origami on SLBs, His$_{10}$-tag ICAM-1 (50440-M08H, Sino Biological) (270 ng mL^{-1}) and His$_{10}$-tag B7-1 (50446-M08H, Sino Biological) (130 ng mL^{-1}) were incubated for 75 min at 24 °C and then rinsed off with PBS. PBS was replaced with HBSS for single molecule imaging (H8264-500 ML, Sigma-Aldrich) and HBSS + 2% FBS for T-cell activation experiments.

Total Internal Reflection Fluorescence (TIRF) Microscopy. TIRF microscopy experiments were performed on a home-built system based on a Zeiss Axiovert 200 microscope equipped with a 100×, NA = 1.46 Plan-Apochromat objective (Zeiss). TIR illumination was achieved by shifting the excitation beam parallel to the optical axis with a mirror mounted on a motorized table. The setup was equipped with a 488 nm diode laser (iBeam smart 488, Toptica), a 532 nm diode-pumped solid state (DPSS) laser (Spectra physics Millennia 6s), and a 647 nm diode laser (Obis LX 647, Coherent). Laser lines were overlaid with an OBIS Galaxy beam combiner (Coherent). Direct analog laser modulation (488 and 647 nm) or an Acousto-optic modulator (Isomet) (532 nm) were used to adjust laser intensities (1−3 kW cm^{-2}) and timings using an in-house developed package implemented in LABVIEW (National Instruments). A dichroic mirror (Di01-R405/488/532/635-25x36, Semrock) was used to separate excitation and emission light. Emitted signals were split into two color channels using an Optosplit II image splitter (Cairn) with a dichroic mirror (DD640-FDi01-25x36, Semrock) and emission filters for each color channel (FF01-550/88-25, ET 570/60, ET 675/50, Chroma) and imaged on the same back-illuminated EM-CCD camera (iXon Ultra, DU897, Andor).

Determination of Functionalization Efficiencies *via* Two-Color Colocalization TIRF Microscopy. To determine the efficiency of a particular functionalization step, two fluorescently labeled interaction partners were used, and the efficiency of functionalization was determined *via* two-color colocalization analysis. All fluorescently labeled interaction partners are listed in Table S2). After functionalization, DNA origami constructs were anchored to SLBs as described above and positions of diffraction-limited spots were determined in both color channels. Single molecules were localized and corrected for chromatic aberrations as described.[37] Detected signal positions were counted as colocalized if signals were within a distance of 240 nm. The starting construct was always assigned color channel 1 (DYE 1); the functionalization to be attached at the particular step was assigned color channel 2 (DYE 2). The fraction of colocalized signals, $f_{\text{coloc }XY}$, where X denotes the construct number and Y denotes the functionalization step (Figures S3−S9), was determined by relating the number of signals in the second color channel (DYE 2) that colocalized with a signal in the first color channel (DYE 1), $N_{\text{coloc }XY}$, to the number of detected signals in the first color channel, $N_{\text{total }XY}$ (eq 1).

$$f_{\text{coloc}XY} = N_{\text{coloc}XY}/N_{\text{total}XY} \tag{1}$$

On the basis of eq 1, the functionalization efficiency of each functionalization step was determined for each construct separately.

Each functionalization step, in turn, was optimized with regard to molar ratios and incubation times *via* two-color colocalization experiments (Tables S3−S9). Once a functionalization step was optimized, these conditions were used as the basis for subsequent steps.

Handle Incorporation. A staple strand fluorescently labeled at its 3′-end with AS635P was used in the assembly process, and DNA origami were prestained with YOYO-1 iodide (YOYO) at a concentration of 1 μg mL^{-1} for 45 min at 24 °C. Excessive YOYO was removed using 100 kDa AmiconUltra centrifugal filters, and DNA origami-bearing SLBs were produced as described above. The fraction of incorporated elongated staple strands, $f_{\text{coloc }11}$, was determined by relating the number of signals in the red color channel (DNA-AS635P) that colocalized with a signal in the blue color channel (YOYO), $N_{\text{coloc }11}$, to the number of detected signals in the blue color channel, $N_{\text{total }11}$ (eq 2).

$$f_{\text{coloc}11} = N_{\text{coloc}11}/N_{\text{total}11} \tag{2}$$

The incorporation of the biotinylated staple strand was determined similarly, with the exception that a handle modified with an Alexa Fluor 647 at its 5′-end and a biotin at its 3′-end (AF647-DNA-bt) was used (eq 3).

$$f_{\text{coloc}21} = N_{\text{coloc}21}/N_{\text{total}21} \tag{3}$$

Construct 1: H57-dSAv. The second modification step (following incorporation of the handle) was the hybridization of a biotinylated oligo to the handle. The fraction of DNA origami carrying a biotin modification, $f_{\text{coloc }12}$, was determined. For this, DNA origami were assembled with a handle modified with AS635P at the 3′-end and biotin at the 3′-end (bt-DNA-AS635P). DNA origami were prestained with YOYO as described above. By relating the number of signals in the red color channel (bt-DNA-AS635P) that colocalized with a signal in the blue color channel (YOYO), $N_{\text{coloc }12}$, to the number of detected blue signals, $N_{\text{total }12}$, $f_{\text{coloc }12}$ could be determined (eq 4).

$$f_{\text{coloc}12} = N_{\text{coloc}12}/N_{\text{total}12} \tag{4}$$

Next, the fraction of DNA origami carrying dSAv for further ligand attachment, $f_{\text{coloc }13}$, was determined. For this, DNA origami labeled with bt-DNA-AS635P were incubated with AF555-conjugated dSAv. The number of green signals (dSAv) that colocalized with a red signal (bt-DNA-AS635P), $N_{\text{coloc }13}$, was divided by the number of red signals, $N_{\text{total }13}$. After correction for the fraction of DNA origami carrying neither biotin nor dSAv, we arrive at the fraction of DNA origami carrying a dSAv (eq 5).

$$f_{\text{coloc}13} = \frac{N_{\text{coloc}13}}{N_{\text{total}13}} f_{\text{coloc}12} \tag{5}$$

Finally, the fraction of DNA origami carrying a TCR ligand, $f_{\text{coloc }14}$, was determined by using DNA origami labeled with bt-DNA-AS635P and AF555-conjugated H57-scF$_V$. By evaluating the number of green signals (H57-scF$_V$) that colocalized with a red signal (bt-DNA-AS635P), $N_{\text{coloc }14}$, divided by the number of red signals ($N_{\text{total }14}$) and corrected for the fraction of unoccupied DNA origami, the fraction of DNA origami functionalized with H57-scF$_V$ could be determined (eq 6).

$$f_{\text{coloc}14} = \frac{N_{\text{coloc}14}}{N_{\text{total}14}} f_{\text{coloc}12} \tag{6}$$

https://doi.org/10.1021/acsnano.1c05411
ACS Nano 2021, 15, 15057−15068

Construct 2: H57-dSAv-NL. The second modification step (following incorporation of the biotinylated handle) concerned the attachment of AF555-labeled dSAv (dSAv-AF555). For this, AF647-DNA-bt was employed as handle. The fraction of biotin-bound dSAv was evaluated by dividing the number of green signals (dSAv-AF555) that colocalized with a red signal (AF647-DNA-bt), $N_{\text{coloc 22}}$, by the number of red signals ($N_{\text{total 22}}$), and this value was corrected for the fraction of unoccupied DNA origami (eq 7).

$$f_{\text{coloc22}} = \frac{N_{\text{coloc22}}}{N_{\text{total22}}} f_{\text{coloc21}} \tag{7}$$

Finally, to determine the fraction of DNA origami functionalized with H57-scF$_V$, DNA origami were prestained with YOYO and AS635P-conjugated H57-scF$_V$ was used for two-color colocalization experiments. The number of red signals (H57-scF$_V$) that colocalized with signals in the blue channel (YOYO), $N_{\text{coloc 23}}$, divided by the number of blue signals ($N_{\text{total 23}}$), yielded the fraction of DNA origami functionalized with H57-scF$_V$ (eq 8).

$$f_{\text{coloc23}} = N_{\text{coloc23}}/N_{\text{total23}} \tag{8}$$

Construct 3: H57-DNA. The second modification step (following incorporation of the handle) concerned the hybridization of a DNA-conjugated H57-scF$_V$ to the handle. An AS635P-modified handle (DNA-AS635P) and AF555-labeled H57-DNA was applied to determine the fraction of DNA origami functionalized with DNA-conjugated H57-scF$_V$ ($f_{\text{coloc 32}}$), The number of green signals (H57-scF$_V$) colocalizing with a red signal (DNA-AS635P), $N_{\text{coloc 32}}$, was divided by the number of red signals ($N_{\text{total 32}}$), and corrected for the fraction of DNA origami without handle, $f_{\text{coloc 11}}$ (eq 9).

$$f_{\text{coloc32}} = \frac{N_{\text{coloc32}}}{N_{\text{total32}}} f_{\text{coloc11}} \tag{9}$$

Construct 4: H57-PNA. The fraction of DNA origami functionalized with PNA-conjugated H57-scF$_V$ ($f_{\text{coloc 42}}$) was determined in analogy to construct H57-DNA (eq 10).

$$f_{\text{coloc42}} = \frac{N_{\text{coloc42}}}{N_{\text{total42}}} f_{\text{coloc11}} \tag{10}$$

Construct 5: H57-mSAv. The second modification step (following incorporation of the handle) was the hybridization of DNA-coupled mSAv to the handle. For determining the fraction of DNA origami functionalized with mSAv-DNA, $f_{\text{coloc 52}}$, DNA origami were prestained with YOYO and AS635P-labeled mSAv-DNA was used. By determining the number of signals in the red color channel (mSAv-DNA-AS635P) that colocalized with a signal in the blue color channel (YOYO), $N_{\text{coloc 52}}$, divided by the number of detected blue signals, $N_{\text{total 52}}$, $f_{\text{coloc 52}}$ could be derived *via* (eq 11).

$$f_{\text{coloc52}} = N_{\text{coloc52}}/N_{\text{total52}} \tag{11}$$

The fraction of DNA origami functionalized with H57-scF$_V$, $f_{\text{coloc 53}}$, was determined by using mSAv-DNA-AS635P and AF555-conjugated H57-scF$_V$. Here, the number of green signals (H57-scF$_V$) that colocalized with a red signal (mSAv-DNA-AS635P), $N_{\text{coloc 53}}$, were divided by the number of red signals ($N_{\text{total 53}}$) and corrected for the fraction of DNA origami without mSAv-DNA, yielding the fraction of DNA origami functionalized with H57-scF$_V$, $f_{\text{coloc 53}}$ (eq 12).

$$f_{\text{coloc53}} = \frac{N_{\text{coloc53}}}{N_{\text{total53}}} f_{\text{coloc52}} \tag{12}$$

Construct 6: H57-tSAv. The first two steps for generating this construct were analogous to those involved in the generation of construct 1: dSAv-H57.

The fraction of DNA origami functionalized with tSAv, $f_{\text{coloc 63}}$, was determined by fluorescently labeling DNA origami with YOYO and using AS635P-labeled tSAv. The number of red signals (tSAv) that colocalized with a blue signal (YOYO), $N_{\text{coloc 63}}$, was divided by the number of blue signals ($N_{\text{total 63}}$). Thus, the fraction of DNA origami functionalized with tSAv is given by eq 13.

$$f_{\text{coloc63}} = N_{\text{coloc63}}/N_{\text{total63}} \tag{13}$$

The fraction of DNA origami functionalized with H57-scF$_V$, $f_{\text{coloc 64}}$, was derived in analogy to eq 6 for H57-dSAv (eq 14).

$$f_{\text{coloc64}} = \frac{N_{\text{coloc64}}}{N_{\text{total64}}} * f_{\text{coloc12}} \tag{14}$$

Construct 7: H57-tSAv-NL. Construct H57-tSAv-NL was created in analogy to H57-dSAv-NL, yielding the fraction of biotin-bound tSAv *via* eq 15.

$$f_{\text{coloc72}} = \frac{N_{\text{coloc72}}}{N_{\text{total72}}} f_{\text{coloc21}} \tag{15}$$

and the fraction of DNA origami functionalized with H57-scF$_V$ *via* eq 16:

$$f_{\text{coloc73}} = N_{\text{coloc73}}/N_{\text{total73}} \tag{16}$$

Determination of Functionalization Stoichiometry *via* Brightness Analysis. Two-color colocalization analysis yielded the fraction of DNA origami carrying at least one H57-scF$_V$. To determine the number of ligands on a functionalized DNA origami construct, we used single molecule brightness analysis based on a MATLAB (Mathworks)-based maximum-likelihood estimator to determine position, integrated brightness B, full width at half-maximum (fwhm), and local background of individual signals in the images as described previously.[38,39] Briefly, functionalized DNA origami were anchored to SLBs, and the integrated brightness B was determined for all recorded positions. Images were taken at multiple different locations ($n \geq 10$) yielding a minimum of ~800 signals. The brightness values B of a monomer reference (a SLB-anchored single H57-scF$_V$ molecule labeled with AF555) were used to calculate the probability density function (pdf) of monomers, $\rho_1(B)$. Because of the independent photon emission process, the corresponding pdfs of N colocalized emitters can be calculated by a series of convolution integrals:

$$\rho_n(B) = \int_1^{\rho} (B')\rho_{N-1}(B - B')\, \mathrm{d}B'. \tag{17}$$

A weighted linear combination of these pdfs was used to calculate the brightness distribution of a mixed population of monomers and oligomers:

$$\rho_n(B) = \sum_{N=1}^{N_{\max}} \alpha_n \rho_n(B). \tag{18}$$

Brightness values for each DNA origami construct were pooled and used to calculate $\rho(B)$. A least-squares fit with eq 18 was employed to determine the weights of the individual pdfs, α_N, with $\sum_{N=1}^{N_{\max}} \alpha_n = 1$. For fits of constructs 1−5, no higher contributions than monomers (α_1) were observed. For fits of construct 6 and 7, contributions up to trimers (α_3) were observed.

Mobility of DNA Origami Constructs on SLBs. For diffusion analysis of DNA origami constructs, at least 10 image sequences with 100 images each were recorded at different locations on the SLB at an illumination time of 3 ms and a time lag of 10 ms. Images were analyzed using in-house algorithms implemented in MATLAB.[40] Mean-square displacements (MSDs) were averaged over all trajectories, plotted as a function of time lag t and the diffusion coefficient D was determined by fitting the function MSD = $4Dt$ + $4\sigma_{xy}$, where σ_{xy} denotes the localization precision; diffusion coefficients were determined from the first two data points of the MSD-t-plot.

Determination of H57-scF$_V$ Surface Densities. Average surface densities of AF555-labeled H57-scF$_V$ on SLBs were determined by dividing mean intensities per μm^2 recorded at eight different positions on the SLB by the brightness of a single AF555-H57-scF$_V$ molecule.

Determination of TCR Surface Densities. Average TCR surface densities were calculated from T-cells in contact with ICAM-1-functionalized SLBs and labeled to saturation with H57-scF$_V$ variants

https://doi.org/10.1021/acsnano.1c05411
ACS Nano 2021, 15, 15057−15068

(DNA-conjugated H57-scF$_V$, PNA-conjugated H57-scF$_V$, biotinylated H57-scF$_V$, H57-scF$_V$) fluorescently labeled with AF555.[37] T-cell brightness per square micrometer was then divided by the brightness of a single AF555-H57-scF$_V$ molecule.

Calcium Imaging Experiments and Analysis. A total of 10^6 T-cells was incubated in T-cell media supplemented with 5 μg mL^{-1} Fura-2 AM (11524766, ThermoFisher Scientific) for 20 min at 24 °C. Excessive Fura-2 AM was removed by washing 3× with HBSS + 2% FBS. T-cells were diluted with HBSS + 2% FBS to get a final concentration of 5 × 10^3 cells μL^{-1}. A 10^5 portion of cells was transferred to the Lab-Tek chamber, and image acquisition was started immediately after T cells landed on the functionalized SLBs. Fura-2 AM was excited using a monochromatic light source (Polychrome V, TILL Photonics), coupled to a Zeiss Axiovert 200 M equipped with a 10× objective (Olympus), 1.6× tube lens, and an Andor iXon Ultra EMCCD camera. A long-pass filter (T400lp, Chroma) and an emission filter were used (510/80ET, Chroma). Imaging was performed with excitation at 340 and 380 nm, with illumination times of 50 and 10 ms, respectively. The total recording time was 10 min at 1 Hz. Precise temperature control was enabled by an in-house-built incubator equipped with a heating unit. Calcium experiments were carried out at 37 °C.

ImageJ was used to generate ratio and sum images of 340 nm/380 nm. T cells were segmented and tracked *via* the sum image of both channels using an in-house Matlab algorithm based on Gao *et al.*[41] Cellular positions and tracks were stored and used for intensity extraction based on the ratio image. Intensity traces were normalized to the starting value at time point zero. Traces were categorized in "activating" and "non-activating" based on an activation threshold ratio of 0.4. The activation threshold was chosen based on comparison of individual traces of a positive control (ICAM-1 100 μm^{-2}, B7-1 100 μm^{-2}, pMHC 150 μm^{-2}) and a negative control (ICAM-1 100 μm^{-2}, B7-1 100 μm^{-2}) ($n > 40$). For generating dose−response curves, at least 15 calcium measurements (of typically ∼100 cells in a region of interest) were conducted, with each measurement at a specific ligand density. The percentage of activated cells was evaluated for each measurement and normalized to the positive control. Data were plotted as % activated cells A as a function of ligand surface densities L to generate dose−response curves and fitted with eq 19 to extract the activation threshold T_A, the maximum response A_{max} and the Hill coefficient n.

$$A = \frac{A_{max}}{1 + 10^{(\log T_A - L)n}} \tag{19}$$

All fit parameters and their 95% confidence intervals (CI) are summarized in the Table S3. Statistical significance between the values $T_{A,1}$ and $T_{A,2}$ for two different data sets was determined *via* a bootstrap ratio test[42,43] as follows: A bootstrap sample was obtained by drawing n data points (sampling with replacement) from a dose−response curve, where n equals the size of the data set. From each data set, 1000 bootstrap samples were drawn and fitted *via* eq 19. This yielded threshold values $T^i_{A,1}$ and $T^i_{A,2}$ (i = 1,···,1000) for each of the bootstrap samples from the two different data sets. The ratio $T^i_{A,1}/T^i_{A,2}$ (i = 1,···,1000) was calculated for each pair of bootstrap samples. If the 100(1−α)% CI of $\log(T^i_{A,1}/T^i_{A,2})$ did not contain 0, the null hypothesis of equal T_A was rejected at a significance level of α.

Protein Expression, Purification, and Conjugation. The TCRβ-reactive H57 single chain antibody fragment (H57-scF$_V$) featuring an unpaired cysteine at the C-terminus (S248C) and the H57-scF$_V$ equipped with a C-terminal BirA ligase biotinylation site were prepared as described.[44,6] Both H57-scF$_V$ versions were cloned into a pET21a(+) expression vector for expression in *Escherichia coli* (BL-21). Insoluble inclusion bodies were extracted *via* sonication and carefully washed with 1% Triton (Merck) and 1% deoxycholic acid (Merck) in 50 mM Tris pH 8.0, 0.2 M NaCl, and 2 mM EDTA (all Merck) before dissolving them finally in 6 M guanidine hydrochloride (Merck). H57-scF$_V$ were refolded from inclusion bodies by a stepwise reduction of the guanidine hydrochloride concentration within the refolding buffer (50 mM Tris pH 8.0, 0.2 M NaCl, 1 mM EDTA) and shifting the redox system from reducing to oxidizing conditions.[45] After a final dialyzing step against 1× PBS, refolded H57-scF$_V$ were concentrated using AmiconUltra-15 centrifugal filters with a 10 kDa cutoff (Merck) and purified *via* gel filtration using Superdex 200 (10/300, Cytiva) on an Äkta pure chromatography system (Cytiva). H57 scF$_V$ containing an unpaired cysteine were concentrated in the presence of 50 μM Tris(2-carboxyethyl) phosphine hydrochloride (TCEP, Pierce).

Monomeric H57-scF$_V$ featuring a BirA recognition site was site-specifically biotinylated using a biotin ligase (Avidity) at 30 °C, followed by a buffer exchange to 1× PBS *via* gel filtration (Superdex-75, 30/300 Cytiva). Biotinylated H57-scF$_V$ was randomly conjugated on surface-exposed lysines with Alexa Fluor 555 (AF555) carboxylic acid, succinimidyl ester (ThermoFisher Scientific), or Abberior Star 635P (AS635P) carboxylic acid, succinimidyl ester (Abberior) according to the manufacturer's instructions. To remove excess dye, the AF555- or AS635P-conjugated and biotinylated H57-scF$_V$ were purified *via* gel filtration using Superdex 75 (10/300 GL, Cytiva). Fractions containing monomeric, fluorescently labeled and biotinylated H57-scF$_V$ were concentrated to 0.2−1 mg/mL with 10 kDa AmiconUltra-4 centrifugal filters (Merck) and stored in 1× PBS supplemented with 50% glycerol at −20 °C. The protein-to-dye ratio ranged between 0.93 and 1.1 for the AF555-labeled H57-scF$_V$ and was 2.0 for the AS635P-labeled H57-scF$_V$ as determined by spectrophotometry (280 to 555 nm or 280 to 638 nm ratio).

H57-scF$_V$ featuring a free cysteine at the C-terminus was conjugated to dibenzyl cyclooctyne-maleimide (DBCO-maleimide, Jena Bioscience) in the presence of 50 μM TCEP for 2 h at room temperature followed by a gel filtration step (Superdex 75, 30/300 Cytiva) to remove unreacted DBCO-maleimide. Directly thereafter, monomeric H57-scF$_V$-DBCO was labeled with AF555 carboxylic acid, succinimidyl ester (ThermoFisher Scientific), and purified *via* gel filtration to remove excess unconjugated dye. In the last step, AF555-conjugated H57-scF$_V$-DBCO was coupled to Azido-PEG4-DNA (TTTTACATGACACTACTCCAC, Biomers) or Azido-PNA (see below) for 2.5 h at room temperature, purified *via* gel filtration (Superdex 75, 30/300 Cytiva) to remove unreacted Azido-PEG4-DNA or Azido-PNA, concentrated with 10 kDa AmiconUltra-4 centrifugal filters (Merck), and stored in 1× PBS supplemented with 50% glycerol at −20 °C. The protein to AF555-dye ratio was 1.1 for the H57-DNA, and 1.15 for the H57-PNA as determined by spectrophotometry (280 to 555 nm ratio) before conjugation to Azido-PEG4-DNA or Azido-PNA. To arrive at Azido-PNA, we functionalized PNA-cysteine (O-TTACATGACACTACTCCAC, Panagene) with Azido-PEG3-maleimide (Jena Bioscience) according to the manufacturer's instructions (Azido-PEG3-Maleimide Preparation Kit). The product was purified *via* reversed phase chromatography (1260 Infinity II, Agilent Technologies) on a C18 column (Pursuit XRs 5 C18 250 mm × 21.2 mm) to separate PNA-cysteine from Azido-PNA. Positive fractions containing only Azido-PNA were verified by MALDI-TOF mass spectrometry (Bruker).

Monovalent streptavidin (mSAv) featuring an unpaired cysteine (A106C) in the biotin-binding subunit was produced as described.[46] After refolding from inclusion bodies and purification *via* anion exchange chromatography (Mono Q, 5/50, Cytiva) and gel filtration (Superdex 200, 30/300, Cytiva), mSAv was labeled randomly on lysine residues with AS635P carboxylic acid, succinimidyl ester (Abberior) according to the manufacturer's instructions and purified *via* gel filtration (Superdex 200, 30/300 Cytiva). Fractions containing STAR635P-conjugated mSAV were concentrated with 10 kDa AmiconUltra-4 centrifugal filters (Merck) and conjugated to trans-cyclooctene-PEG3-maleimide (TCO-PEG3-maleimide, Jena Bioscience) and again purified *via* gel filtration (Superdex 200, 30/300, Cytiva) to remove unreacted TCO-PEG3-maleimide. Finally, AS635P-labeled mSAv-TCO was conjugated to a tetrazine-PEG5-oligo (TTTTACATGACACTACTCCAC, Biomers) for 2 h at room temperature and purified *via* gel filtration (Superdex 75, 30/300, Cytiva). Monomeric STAR635P-labeled mSAv-DNA was concentrated with 10 kDa AmiconUltra-4 centrifugal filters (Merck) and stored in 1× PBS supplemented with 50% glycerol at −20 °C. The

https://doi.org/10.1021/acsnano.1c05411
ACS Nano 2021, 15, 15057−15068

protein-to-dye ratio for the AS635P-labeled mSAv-DNA was 1.0 as determined by spectrophotometry (280 to 638 nm ratio) before conjugation with TCO-PEG3-maleimide.

Trans-divalent streptavidin (dSAv) and tetravalent streptavidin (tSAv) were prepared based on a protocol by Fairhead *et al.*[27] and as described in Hellmeier *et al.*[6]

Tetravalent streptavidin was refolded from inclusion bodies containing only biotin-binding streptavidin subunits and purified *via* gel filtration (Superdex 200, 30/300, Cytiva). Monomeric fractions were labeled with Abberior Star 635P (AS635P) carboxylic acid, succinimidyl ester (Abberior) according to the manufacturer's instructions and purified *via* gel filtration (Superdex 200, 30/300 Cytiva). Fractions containing STAR635P-conjugated mSAv were concentrated with 10 kDa AmiconUltra-4 centrifugal filters (Merck) and stored in 1× PBS supplemented with 50% glycerol at −20 °C. The protein-to-dye ratio for the AS635P-labeled tSAv was 1.2 as determined by spectrophotometry (280 to 638 nm ratio). 2xHis_6-tag pMHC-AF555 was produced as described.[37]

Tissue Culture. Primary T-cells isolated from lymph nodes or spleen of 5c.c7 $\alpha\beta$ TCR transgenic mice were pulsed with 0.5 μM moth cytochrome c peptide (MCC) 88-103 peptide (C18-reverse phase HPLC-purified; sequence: ANERADLIAYLKQATK, T-cell epitope underlined, Elim Biopharmaceuticals Inc., USA) and 50 U ml^{-1} IL-2 (eBioscience) for 7 days to expand CD4+ T-cells and arrive at an antigen-experienced T-cell culture.[47] T-cells were maintained at 37 °C and 5% CO_2 in RPMI 1640 media (Life Technologies) supplemented with 10% FBS (Merck), 100 μg mL^{-1} penicillin (Life Technologies), 100 μg mL^{-1} streptomycin (Life Technologies), 2 mM L-glutamine (Life Technologies), 0.1 mM nonessential amino acids (Lonza), 1 mM sodium pyruvate (Life Technologies) and 50 μM β-mercaptoethanol (Life Technologies). Dead cells were removed 6 days after T-cell isolation with a density-dependent gradient centrifugation step (Histopaque 1119, Sigma). Antigen-experienced T-cells were used for experiments on day 7−9.

Animal Model and Ethical Compliance Statement. The 5c.c7 $\alpha\beta$ TCR-transgenic mice bred onto the B10.A background were a kind gift from Michael Dustin (University of Oxford,UK). Both male and female mice at 8−12 weeks old were randomly selected and sacrificed for isolation of T-cells from lymph nodes and spleen, which was evaluated by the ethics committees of the Medical University of Vienna and approved by the Federal Ministry of Science, Research and Economy, BMWFW (BMWFW-66.009/0378-WF/V/3b/2016). Animal husbandry, breeding, and sacrifice of mice were performed in accordance to Austrian law (Federal Ministry for Science and Research, Vienna, Austria), the guidelines of the ethics committees of the Medical University of Vienna, and the guidelines of the Federation of Laboratory Animal Science Associations (FELASA), which match those of Animal Research: Reporting *in vivo* Experiments (ARRIVE). Further, animal husbandry, breeding, and sacrifice for T-cell isolation was conducted under Project License (I4BD9B9A8L) which was evaluated by the Animal Welfare and Ethical Review Body of the University of Oxford and approved by the Secretary of State of the UK Home Department. They were performed in accordance with the Animals (Scientific Procedures) Act 1986, the guidelines of the ethics committees of the Medical Science of University of Oxford, and the guidelines of the Federation of Laboratory Animal Science Associations (FELASA), which match those of Animal Research: Reporting *in vivo* Experiments (ARRIVE).

ASSOCIATED CONTENT

Supporting Information

The Supporting Information is available free of charge at https://pubs.acs.org/doi/10.1021/acsnano.1c05411.

Diffusion coefficients of constructs on SLBs; fluorophore pairs used for two-color colocalization microscopy; optimization of functionalization conditions; functionalization efficiencies; number of H57-scFV molecules per DNA origami construct; fitting parameters of fits to dose−response curves; list of used oligonucleotides; additional figures supporting the text (PDF)

AUTHOR INFORMATION

Corresponding Authors

Joschka Hellmeier − *Institute of Applied Physics, TU Wien, Vienna 1060, Austria*; Email: hellmeier@iap.tuwien.ac.at

Eva Sevcsik − *Institute of Applied Physics, TU Wien, Vienna 1060, Austria*; orcid.org/0000-0002-2155-1675; Email: eva.sevcsik@tuwien.ac.at

Authors

René Platzer − *Center for Pathophysiology, Infectiology and Immunology, Institute for Hygiene and Applied Immunology, Medical University of Vienna, Vienna 1090, Austria*

Vanessa Mühlgrabner − *Center for Pathophysiology, Infectiology and Immunology, Institute for Hygiene and Applied Immunology, Medical University of Vienna, Vienna 1090, Austria*

Magdalena C. Schneider − *Institute of Applied Physics, TU Wien, Vienna 1060, Austria*

Elke Kurz − *Kennedy Institute of Rheumatology, University of Oxford, Oxford OX3 7FY, U.K.*

Gerhard J. Schütz − *Institute of Applied Physics, TU Wien, Vienna 1060, Austria*; orcid.org/0000-0003-1542-1089

Johannes B. Huppa − *Center for Pathophysiology, Infectiology and Immunology, Institute for Hygiene and Applied Immunology, Medical University of Vienna, Vienna 1090, Austria*

Complete contact information is available at: https://pubs.acs.org/10.1021/acsnano.1c05411

Notes

The authors declare no competing financial interest.

An earlier version of this work was uploaded to a preprint server: Hellmeier, J.; Platzer, R.; Mühlgrabner, V.; Schneider, M. C.; Kurz, E.; Schütz, G. J.; Huppa, J. B.; Sevcsik, E. Strategies for the Site-Specific Decoration of DNA Origami Nanostructures with Functionally Intact Proteins. 2021, 07.01.450695. bioRxiv. 10.1101/2021.07.01.450695 (accessed August 21, 2021).

ACKNOWLEDGMENTS

This work was supported by the Austrian Science Fund (FWF Projects V538-B26 (E.S.), T134040-2010 (J.H.) and F6809-N36 (G.J.S., M.C.S.); the Ph.D. program Cell Communication in Health and Disease W1205, R.P., J.B.H.), the TU Wien doctoral college BioInterface (J.H.), the Vienna Science and Technology Fund (WWTF, LS13-030, G.J.S. and J.B.H.), the Boehringer Ingelheim Fonds (R.P.), the Wellcome Trust (Principal Research Fellowship 100262 Z/12/Z, E.K.) and the Kennedy Trust for Rheumatology Research (E.K.).

REFERENCES

(1) Rothemund, P. W. K. Folding DNA to Create Nanoscale Shapes and Patterns. *Nature* **2006**, *440* (7082), 297−302.

(2) Shaw, A.; Lundin, V.; Petrova, E.; Fördős, F.; Benson, E.; Al-Amin, A.; Herland, A.; Blokzijl, A.; Högberg, B.; Teixeira, A. I. Spatial Control of Membrane Receptor Function Using Ligand Nanocalipers. *Nat. Methods* **2014**, *11* (8), 841−846.

(3) Veneziano, R.; Moyer, T. J.; Stone, M. B.; Wamhoff, E. C.; Read, B. J.; Mukherjee, S.; Shepherd, T. R.; Das, J.; Schief, W. R.; Irvine, D. J.; Bathe, M. Role of Nanoscale Antigen Organization on B-Cell

Activation Probed Using DNA Origami. *Nat. Nanotechnol.* **2020**, *15*, 716−723.
(4) Huang, D.; Patel, K.; Perez-Garrido, S.; Marshall, J. F.; Palma, M. DNA Origami Nanoarrays for Multivalent Investigations of Cancer Cell Spreading with Nanoscale Spatial Resolution and Single-Molecule Control. *ACS Nano* **2019**, *13*, 728−736.
(5) Angelin, A.; Weigel, S.; Garrecht, R.; Meyer, R.; Bauer, J.; Kumar, R. K.; Hirtz, M.; Niemeyer, C. M. Multiscale Origami Structures as Interface for Cells. *Angew. Chem., Int. Ed.* **2015**, *54* (52), 15813−15817.
(6) Hellmeier, J.; Platzer, R.; Eklund, A. S.; Schlichthaerle, T.; Karner, A.; Motsch, V.; Schneider, M. C.; Kurz, E.; Bamieh, V.; Brameshuber, M.; Preiner, J.; Jungmann, R.; Stockinger, H.; Schütz, G. J.; Huppa, J. B.; Sevcsik, E. DNA Origami Demonstrate the Unique Stimulatory Power of Single PMHCs as T Cell Antigens. *Proc. Natl. Acad. Sci. U. S. A.* **2021**, *118* (4), No. e2016857118.
(7) Berger, R. M. L.; Weck, J. M.; Kempe, S. M.; Hill, O.; Liedl, T.; Rädler, J. O.; Monzel, C.; Heuer-jungemann, A. Nanoscale FasL Organization on DNA Origami to Decipher Apoptosis Signal Activation in Cells. *Small* **2021**, *17*, 2101678.
(8) Teixeira, A. I.; Fang, T.; Alvelid, J.; Spratt, J.; Ambrosetti, E.; Testa, I. Spatial Regulation of T-Cell Signaling by Programmed Death-Ligand 1 on Wireframe DNA Origami Flat Sheets. *ACS Nano* **2021**, *15* (2), 3441−3452.
(9) Garrecht, R.; Meyer, R.; Duppach, J.; Reipschläger, S.; Watzl, C.; Niemeyer, C. M. Designed DNA Surfaces for *in Vitro* Modulation of Natural Killer Cells. *ChemBioChem* **2016**, *17* (6), 486−492.
(10) Fu, J.; Liu, M.; Liu, Y.; Woodbury, N. W.; Yan, H. Interenzyme Substrate Diffusion for an Enzyme Cascade Organized on Spatially Addressable DNA Nanostructures. *J. Am. Chem. Soc.* **2012**, *134* (12), 5516−5519.
(11) Fu, J.; Yang, Y. R.; Johnson-Buck, A.; Liu, M.; Liu, Y.; Walter, N. G.; Woodbury, N. W.; Yan, H. Multi-Enzyme Complexes on DNA Scaffolds Capable of Substrate Channelling with an Artificial Swinging Arm. *Nat. Nanotechnol.* **2014**, *9* (7), 531−536.
(12) Li, S.; Jiang, Q.; Liu, S.; Zhang, Y.; Tian, Y.; Song, C.; Wang, J.; Zou, Y.; Anderson, G. J.; Han, J. Y.; Chang, Y.; Liu, Y.; Zhang, C.; Chen, L.; Zhou, G.; Nie, G.; Yan, H.; Ding, B.; Zhao, Y. A DNA Nanorobot Functions as a Cancer Therapeutic in Response to a Molecular Trigger *in Vivo*. *Nat. Biotechnol.* **2018**, *36* (3), 258−264.
(13) Engelen, W.; Dietz, H. Advancing Biophysics Using DNA Origami. *Annu. Rev. Biophys.* **2021**, *50*, 469−492.
(14) Koßmann, K. J.; Ziegler, C.; Angelin, A.; Meyer, R.; Skoupi, M.; Rabe, K. S.; Niemeyer, C. M. A Rationally Designed Connector for Assembly of Protein-Functionalized DNA Nanostructures. *ChemBioChem* **2016**, *17*, 1102−1106.
(15) Timm, C.; Niemeyer, C. M. Assembly and Purification of Enzyme-Functionalized DNA Origami Structures. *Angew. Chem., Int. Ed.* **2015**, *54* (23), 6745−6750.
(16) Vogele, K.; List, J.; Simmel, F. C.; Pirzer, T. Enhanced Efficiency of an Enzyme Cascade on DNA-Activated Silica Surfaces. *Langmuir* **2018**, *34* (49), 14780−14786.
(17) Zhang, Y.; Tsitkov, S.; Hess, H. Proximity Does Not Contribute to Activity Enhancement in the Glucose Oxidase-Horseradish Peroxidase Cascade. *Nat. Commun.* **2016**, *7*, 13982.
(18) Glettenberg, M.; Niemeyer, C. M. Tuning of Peroxidase Activity by Covalently Tethered DNA Oligonucleotides. *Bioconjugate Chem.* **2009**, *20* (5), 969−975.
(19) Fruk, L.; Müller, J.; Niemeyer, C. M. Kinetic Analysis of Semisynthetic Peroxidase Enzymes Containing a Covalent DNA-Heme Adduct as the Cofactor. *Chem. - Eur. J.* **2006**, *12* (28), 7448−7457.
(20) Keppler, A.; Gendreizig, S.; Gronemeyer, T.; Pick, H.; Vogel, H.; Johnsson, K. A General Method for the Covalent Labeling of Fusion Proteins with Small Molecules *in Vivo*. *Nat. Biotechnol.* **2003**, *21* (1), 86−89.
(21) Los, G. V.; Encell, L. P.; McDougall, M. G.; Hartzell, D. D.; Karassina, N.; Zimprich, C.; Wood, M. G.; Learish, R.; Ohana, R. F.; Urh, M.; Simpson, D.; Mendez, J.; Zimmerman, K.; Otto, P.; Vidugiris, G.; Zhu, J.; Darzins, A.; Klaubert, D. H.; Bulleit, R. F.; Wood, K. V. HaloTag: A Novel Protein Labeling Technology for Cell Imaging and Protein Analysis. *ACS Chem. Biol.* **2008**, *3* (6), 373−382.
(22) Sagredo, S.; Pirzer, T.; AghebatRafat, A.; Goetzfried, M. A.; Moncalian, G.; Simmel, F. C.; De La Cruz, F. Orthogonal Protein Assembly on DNA Nanostructures Using Relaxases. *Angew. Chem., Int. Ed.* **2016**, *55* (13), 4348−4352.
(23) Saccà, B.; Meyer, R.; Erkelenz, M.; Kiko, K.; Arndt, A.; Schroeder, H.; Rabe, K. S.; Niemeyer, C. M. Orthogonal Protein Decoration of DNA Origami. *Angew. Chem., Int. Ed.* **2010**, *49* (49), 9378−9383.
(24) Yamazaki, T.; Heddle, J. G.; Kuzuya, A.; Komiyama, M. Orthogonal Enzyme Arrays on a DNA Origami Scaffold Bearing Size-Tunable Wells. *Nanoscale* **2014**, *6* (15), 9122−9126.
(25) Wu, N.; Czajkowsky, D. M.; Zhang, J.; Qu, J.; Ye, M.; Zeng, D.; Zhou, X.; Hu, J.; Shao, Z.; Li, B.; Fan, C. Molecular Threading and Tunable Molecular Recognition on DNA Origami Nanostructures. *J. Am. Chem. Soc.* **2013**, *135* (33), 12172−12175.
(26) Voigt, N. V.; Tørring, T.; Rotaru, A.; Jacobsen, M. F.; Ravnsbæk, J. B.; Subramani, R.; Mamdouh, W.; Kjems, J.; Mokhir, A.; Besenbacher, F.; Gothelf, K. V. Single-Molecule Chemical Reactions on DNA Origami. *Nat. Nanotechnol.* **2010**, *5* (3), 200−203.
(27) Fairhead, M.; Krndija, D.; Lowe, E. D.; Howarth, M. Plug-and-Play Pairing *via* Defined Divalent Streptavidins. *J. Mol. Biol.* **2014**, *426* (1), 199−214.
(28) Langecker, M.; Arnaut, V.; Martin, T. G.; List, J.; Renner, S.; Mayer, M.; Dietz, H.; Simmel, F. C. Synthetic Lipid Membrane Channels Formed by Designed DNA Nanostructures. *Science (Washington, DC, U. S.)* **2012**, *338* (6109), 932−936.
(29) Huppa, J. B.; Axmann, M.; Mörtelmaier, M. A.; Lillemeier, B. F.; Newell, E. W.; Brameshuber, M.; Klein, L. O.; Schütz, G. J.; Davis, M. M. TCR-Peptide-MHC Interactions *in Situ* Show Accelerated Kinetics and Increased Affinity. *Nature* **2010**, *463* (7283), 963−967.
(30) Lin, J. J.; O'Donoghue, G. P.; Wilhelm, K. B.; Coyle, M. P.; Low-Nam, S. T.; Fay, N. C.; Alfieri, K. N.; Groves, J. T. Membrane Association Transforms an Inert Anti-TCRβ Fab' Ligand into a Potent T Cell Receptor Agonist. *Biophys. J.* **2020**, *118*, 2879−2893.
(31) Strauss, M. T.; Schueder, F.; Haas, D.; Nickels, P. C.; Jungmann, R. Quantifying Absolute Addressability in DNA Origami with Molecular Resolution. *Nat. Commun.* **2018**, *9* (2018), 1600.
(32) Taylor, M. J.; Husain, K.; Gartner, Z. J.; Mayor, S.; Vale, R. D. A DNA-Based T Cell Receptor Reveals a Role for Receptor Clustering in Ligand Discrimination. *Cell* **2017**, *169* (1), 108−119.
(33) Zadeh, J. N.; Steenberg, C. D.; Bois, J. S.; Wolfe, B. R.; Pierce, M. B.; Khan, A. R.; Dirks, R. M.; Pierce, N. A. NUPACK: Analysis and Design of Nucleic Acid Systems. *J. Comput. Chem.* **2011**, *32* (1), 170−173.
(34) Nielsen, P. E.; Egholm, M.; Berg, R. H.; Buchardt, O. Sequence-Selective Recognition of DNA by Strand Displacement with a Thymine-Substituted Polyamide. *Science (Washington, DC, U. S.)* **1991**, *254* (5037), 1497−1500.
(35) Cai, H.; Muller, J.; Depoil, D.; Mayya, V.; Sheetz, M. P.; Dustin, M. L.; Wind, S. J. Full Control of Ligand Positioning Reveals Spatial Thresholds for T Cell Receptor Triggering. *Nat. Nanotechnol.* **2018**, *13*, 610−617.
(36) Axmann, M.; Schütz, G. J.; Huppa, J. B. Measuring TCR-PMHC Binding *in Situ* Using a FRET-Based Microscopy Assay. *J. Visualized Exp.* **2015**, *104*, 1−17.
(37) Brameshuber, M.; Kellner, F.; Rossboth, B. K.; Ta, H.; Alge, K.; Sevcsik, E.; Göhring, J.; Axmann, M.; Baumgart, F.; Gascoigne, N. R. J.; Davis, S. J.; Stockinger, H.; Schütz, G. J.; Huppa, J. B. Monomeric TCRs Drive T Cell Antigen Recognition. *Nat. Immunol.* **2018**, *19*, 487−496.
(38) Moertelmaier, M.; Brameshuber, M.; Linimeier, M.; Schütz, G. J.; Stockinger, H. Thinning out Clusters While Conserving Stoichiometry of Labeling. *Appl. Phys. Lett.* **2005**, *87* (26), 1−3.
(39) Schmidt, T.; Schutz, G. J.; Gruber, H. J.; Schindler, H. Local Stoichiometries Determined by Counting Individual Molecules. *Anal. Chem.* **1996**, *68* (24), 4397−4401.

https://doi.org/10.1021/acsnano.1c05411
ACS Nano 2021, 15, 15057−15068

(40) Wieser, S.; Moertelmaier, M.; Fuertbauer, E.; Stockinger, H.; Schütz, G. J. (Un)Confined Diffusion of CD59 in the Plasma Membrane Determined by High-Resolution Single Molecule Microscopy. *Biophys. J.* **2007**, *92* (10), 3719−3728.
(41) Gao, Y.; Kilfoil, M. L. Kilfoil. Accurate Detection and Complete Tracking of Large Populations of Features in Three Dimensions. *Opt. Express* **2009**, *17* (6), 4685−4704.
(42) MacKinnon, J. G. Bootstrap Hypothesis Testing. In *Handbook of Computational Econometrics*; Belsley, D. A., Kontoghiorghes, E. J., Eds.; John Wiley & Sons, Ltd: Chichester, 2009; pp 183−213.
(43) Wheeler, M. W.; Park, R. M.; Bailer, A. J. Comparing Median Lethal Concentration Values Using Confidence Interval Overlap or Ratio Tests. *Environ. Toxicol. Chem.* **2006**, *25* (5), 1441.
(44) Göhring, J.; Kellner, F.; Schrangl, L.; Platzer, R.; Klotzsch, E.; Stockinger, H.; Huppa, J. B.; Schütz, G. J. Temporal Analysis of T-Cell Receptor-Imposed Forces *via* Quantitative Single Molecule FRET Measurements. *Nat. Commun.* **2021**, *12*, 2502.
(45) Tsumoto, K.; Shinoki, K.; Kondo, H.; Uchikawa, M.; Juji, T.; Kumagai, I. Highly Efficient Recovery of Functional Single-Chain Fv Fragments from Inclusion Bodies Overexpressed in Escherichia Coli by Controlled Introduction of Oxidizing Reagent - Application to a Human Single-Chain Fv Fragment. *J. Immunol. Methods* **1998**, *219* (1−2), 119−129.
(46) Platzer, R.; Rossboth, B. K.; Schneider, M. C.; Sevcsik, E.; Baumgart, F.; Stockinger, H.; Schütz, G. J.; Huppa, J. B.; Brameshuber, M. Unscrambling Fluorophore Blinking for Comprehensive Cluster Detection *via* Photoactivated Localization Microscopy. *Nat. Commun.* **2020**, *11*, 4993.
(47) Huppa, J. B.; Gleimer, M.; Sumen, C.; Davis, M. M. Continuous T Cell Receptor Signaling Required for Synapse Maintenance and Full Effector Potential. *Nat. Immunol.* **2003**, *4* (8), 749−755.
(48) Brameshuber, M.; Weghuber, J.; Ruprecht, V.; Gombos, I.; Horváth, I.; Vigh, L.; Eckerstorfer, P.; Kiss, E.; Stockinger, H.; Schütz, G. J. Imaging of Mobile Long-Lived Nanoplatforms in the Live Cell Plasma Membrane. *J. Biol. Chem.* **2010**, *285* (53), 41765−41771.

https://doi.org/10.1021/acsnano.1c05411
ACS Nano 2021, 15, 15057−15068